A&A 534, A47 (2011)
DOI: 10.1051/0004-6361/201116790

Astronomy & Astrophysics

Statistical properties of superactive regions during solar cycles 19–23⋆

A. Q. Chen[1,2], J. X. Wang[1], J. W. Li[2], J. Feynman[3], and J. Zhang[1]

[1] Key Laboratory of Solar Activity of Chinese Academy of Sciences, National Astronomical Observatories, Chinese Academy of Sciences, PR China
e-mail: chenanqin@cma.gov.cn; wangjx@nao.cas.cn
[2] National Center for Space Weather, China Meteorological Administration, PR China
[3] Helio research, 5212 Maryland Avenue, La Crescenta, USA

Received 26 February 2011 / Accepted 20 August 2011

ABSTRACT

Context. Each solar activity cycle is characterized by a small number of superactive regions (SARs) that produce the most violent of space weather events with the greatest disastrous influence on our living environment.
Aims. We aim to re-parameterize the SARs and study the latitudinal and longitudinal distributions of SARs.
Methods. We select 45 SARs in solar cycles 21–23, according to the following four parameters: 1) the maximum area of sunspot group, 2) the soft X-ray flare index, 3) the 10.7 cm radio peak flux, and 4) the variation in the total solar irradiance. Another 120 SARs given by previous studies of solar cycles 19–23 are also included. The latitudinal and longitudinal distributions of the 165 SARs in both the Carrington frame and the dynamic reference frame during solar cycles 19–23 are studied statistically.
Results. Our results indicate that these 45 SARs produced 44% of all the X class X-ray flares during solar cycles 21–23, and that all the SARs are likely to produce a very fast CME. The latitudinal distributions of SARs display the Maunder butterfly diagrams and SARs occur preferentially in the maximum period of each solar cycle. Northern hemisphere SARs dominated in solar cycles 19 and 20 and southern hemisphere SARs dominated in solar cycles 21 and 22. In solar cycle 23, however, SARs occurred about equally in each hemisphere. There are two active longitudes in both the northern and southern hemispheres, about 160°–200° apart. Applying the improved dynamic reference frame to SARs, we find that SARs rotate faster than the Carrington rate and there is no significant difference between the two hemispheres. The synodic periods are 27.19 days and 27.25 days for the northern and southern hemispheres, respectively. The longitudinal distribution of SARs is significantly non-axisymmetric and about 75% SARs occurred near two active longitudes with half widths of 45°.

Key words. Sun: activity – Sun: rotation – sunspots

1. Introduction

Solar active regions (ARs) are the main source of disastrous space weather events in Earth's orbit. Each solar cycle is characterized by a few superactive regions (SARs) that are capable of producing the most violent events with the greatest known disastrous influence on our living environment. It is known that more than 40% of all the major flares are produced by fewer than 0.5% of ARs, which are referred to as SARs in each solar cycle (Bai 1987, 1988; Wang et al. 2011). After the last SAR in a solar cycle is completed, the cycle emission begins to diminish, hence to quantify and parameterize the cycle properties of SARs are of great help for space weather prediction.

The concept of *"superactive region"* was first proposed by Bai (1987). He defined major flares as those with hard X-ray peak fluxes exceeding 1000 counts s^{-1} and studied the major flares observed by the Solar Maximum Mission during 1980–1985. If an AR produced five or more major flares, it would be called a SAR. He found that 28 SARs produced 234 major flares, accounting for 53% of all the major flares during this period. By extending the sample, Bai (1988) analyzed the major flares observed during the period from January 1955 to August 1985, and identified each SAR that produced four or more major flares. In his study, he selected major flares with the following criteria. For solar cycle 19, he selected major flares with comprehensive flare indices (CFI) > 5 (Dodson & Hedeman 1971). For cycle 20 and the early part of cycle 21, he selected major flares with CFI > 6 (Dodson & Hedeman 1971, 1975b, 1981). For the later part of cycle 21, he selected major flares as in his earlier work (Bai 1987). He found that 100 SARs produced 46% of all the major flares in solar cycles 19–21 and that these SARs appeared more frequently in some areas that were called either "hot spots" or "active zones" on the Sun.

Wu & Zhang (1995) and Li & Wang (1997) studied the most violent ARs (SARs) in solar cycles 22 and 21, respectively. Wu & Zhang (1995) had selected 13 SARs in solar cycle 22 based on five parameters: the maximum area of the sunspot group, the index of the X class X-ray flare, the maximum 10.7 cm radio flux, the short-term total solar irradiance decrease, and the maximum proton flux. A total of 16 SARs in solar cycle 21 were chosen by Li & Wang (1997), who used the parameters as in Wu & Zhang (1995) except for the short-term total solar irradiance decrease. The magnetic properties of the most violent SARs (VSARs) in solar cycles 22 and 23 were studied by Tian et al. (2002). They chose 14 SARs in solar cycle 22 and 15 SARs in solar cycle 23 that all produced major flares and/or major solar storms. Among them, 13 VSARs in solar cycle 22 and 12 VSARs in

⋆ Appendix A is available in electronic form at http://www.aanda.org

solar cycle 23 were selected based on the following five parameters: the largest area of sunspot, the soft X-ray flare index, the 10.7 cm radio peak flux, the high-energy proton flux, and the geomagnetic A_p index. They found that most VSARs had net magnetic fluxes higher than 10^{21} Mx, had abnormal magnetic structures, and followed the hemispheric helicity rule. Romano & Zuccarello (2007) presented a statistical analysis of the photospheric magnetic flux evolution of 26 SARs, which reached a flare index larger than 500 (Li et al. 2004) during 2000–2006, and found that the most intense phases of activity were associated with phases of emergence of a magnetic field or flux cancellation. In our preliminary study of Wang et al. (2011), we selected 48 SARs in the last three solar cycles and analyzed the vector magnetic field characteristics of SARs. The selection was made based on five criterion conditions, including the short-term total solar irradiance decrease and an additional four criterion conditions similar to those of Tian et al. (2002), except for the geomagnetic A_p index. Since different parameters were used to parameterize SARs by different authors (Bai 1987, 1988; Wu & Zhang 1995; Li & Wang 1997; Tian et al. 2002; Romano & Zuccarello 2007; Wang et al. 2011), we try in this present paper to select an adequate set of criterion parameters and re-parameterize the SARs in the last three solar cycles. This is only the first step of a sequence of stages. As soon as the SARs are selected based on a unique set of parameters, we first examine statistically the characteristics of the SAR distribution in longitude and latitude. Major efforts are then made to quantify the properties of SARs with vector magnetic-field measurements with the purpose of understanding why the SARs are superactive.

The north-south (N-S) asymmetries of several manifestations of solar activity during solar cycles 19–23 has been studied by many authors. Garcia (1990) studied the N-S asymmetry of large X-ray flares during solar cycles 20 and 21, and found that large flares occur preferentially in the northern hemisphere in the early part and then move to the southern hemisphere as the cycle progresses. Li et al. (1998) found that large X-ray flares occur predominantly in the southern hemisphere in the N-S asymmetry during solar cycle 22. During solar cycles 19–23, The N-S asymmetries of sunspot areas, solar flares, and solar active prominences were studied by Verma (2000). He found that these solar active phenomena occurred primarily in the northern hemisphere during solar cycles 19 and 20 and then in the southern hemisphere during solar cycles 21–23. During solar cycles 21–23, a similar finding was made by Joshi et al. (2010). A theoretical study of the cause of the hemispheric asymmetry was made based on the Babcock-Leighton dynamo model by Ashish & Choudhuri (2009).

The question of whether ARs occur preferentially at some longitudes has been studied by many authors (Švestka 1970; Dodson & Hedeman 1975a; Bai 1988; Tian et al. 2002), who reported evidence that ARs do not occur uniformly over all longitudes but preferentially at some longitudes during some time intervals. These studies, however, were unable to unambiguously identify the active longitudes because the ARs studied occurred during different time intervals. Neugebauer et al. (2000) presented evidence of active longitudes in the solar wind. Ruzmaikin et al. (2001) and Henney & Harvery (2002) identified solar active longitudes in solar magnetograms and related the results to solar non-axisymmetric magnetic fields. The terminology of activity complex and active nests were also used to describe the clustering tendencies of flare-prolific ARs in longitude and latitude (Gaizauskas et al. 1983).

Using two different filtering techniques, Berdyugina & Usoskin (2003) analyzed the sunspot group data for the past 120 years and found that sunspots were formed preferentially in two persistent active longitudes separated by 180° in both the northern and southern hemispheres. Another important conclusion of these authors is that the active longitudes are not fixed in the Carrington system, but continuously migrate in longitude with a variable rate caused by the solar differential rotation. Usoskin et al. (2005) introduced a new method to remove the solar differential rotation of the raw data, which was the same as that used by Berdyugina & Usoskin (2003), without any preprocessing or filtering and confirmed the finding of Berdyugina & Usoskin (2003). Zhang et al. (2007a,b, 2011) used this method and the improved one to study the distribution of solar X-ray flares, respectively. They also found that there were two persistent active longitudes during the last three solar cycles. In this paper, we use the improved method of Zhang et al. (2008, 2011) to calculate the rotation parameters and study the longitudinal distribution of SARs.

This paper is arranged as follows. We describe the parameterization of solar SARs in Sect. 2. We discuss the statistical properties of SARs in Sect. 3, and both our conclusions and discussion in Sect. 4.

2. Parameterizing solar SARs

Different authors adopted very different ways of parameterizing SARs. On the basis of their experiences, we make the following considerations. First, the parameters selected to parameterize SAR should be mostly independent, each providing a complementary insight into SAR physics. Secondly, the parameters should be easy to access, have a long time-interval coverage, and be contained in a database with standard calibrations. Thirdly, the number of parameters should be as small as possible to ensure that the selection of SARs is both simple and unique. The parameters employed to parameterize a SAR in this paper are (1) the maximum area of the sunspot groups, (2) the soft X-ray flare index, (3) the 10.7 cm radio peak flux, and (4) the short-term total solar irradiance decrease (ΔTSI). All or part of them have been used to parameterize the SARs by other authors (Bai 1987, 1988; Wu & Zhang 1995; Li & Wang 1997; Tian et al. 2002; Romano & Zuccarello 2007; Wang et al. 2011). We derive the data that we analyze from the National Geophysical Data Center[1], the Space Weather Prediction Center[2] and the Marshall Space Flight Center[3]. We postpone the use of the CME speed as a potential parameter to future work, that is the use of the linear speed obtained from the CME catalog[4]. In this paper, we assume that the time of a SAR is equal to the central meridian passage time. Our justifications for adopting all four of the aforementioned parameters are discussed below.

The maximum area of the sunspot group indicates the size of the sunspot group. The larger a sunspot group area is, the more likely the group is to have a complex magnetic field and produce major flares and other solar activities (Sammis et al. 2000). The sunspot dynamics, e.g., fast rotation, and strong magnetic shear in the related AR are of course important factors that determine the productivity of major flares (Yan et al. 2009). The soft X-ray flare index indicates how prolific the ARs are in producing major flares. Flares are the sudden release of magnetic energy stored in

[1] ftp://ngdc.noaa.ogv/STP/SOLAR_DATA
[2] http://swpc.noaa.gov
[3] http://solarscience.msfc.nasa.gov/greenwch.shtml
[4] http://cdaw.gsfc.nasa.gov/CME_list

Table 1. The four criterion conditions used to parameterize a SAR.

Criterion condition	Value
Maximum sunspot area	>1000 μh
Flare index	>10.0
10.7 cm peak flux	>1000 s.f.u.
ΔTSI	<−0.1%

the non-potential AR magnetic field, and soft X-ray emission can be detected at this stage. The radiation observed in the soft X-ray wave band reflects the thermal characteristics of the AR's corona. Solar radio impulsive bursts at 10.7 cm are generated by non-thermal processes related to the passage of highly energetic particles from ARs (Covington & Harvey 1958; Covington 1959; Balachandran et al. 2001), and indicate how strong the magnetic fields are for creating the non-thermal emissions. The short-term ΔTSI, which is mostly caused by ARs (Solanki & Flige 2002; Withbroe 2009), is an important criterion variable. It relates the Sun to stars in general because the SARs on the Sun are probably similar to the star spots observed in stellar astronomy.

It is well-known that some ARs persist for several solar rotation periods, but at each passage new AR numbers are assigned. Our study is based on the NOAA AR number. We studied about 10200 ARs in solar cycles 21–23. We refer to an AR as a SAR, if three of the four criterion conditions listed in Table 1 are fulfilled. The soft X-ray flare index is the sum of the numerical multipliers of M and X class X-ray flares for the disk transit of the AR, e.g., 0.1 for an M1 class flare and 1.0 for an X1 class flare. In addition, since solar flares are one of the most representative forms of solar activity and some authors (Bai 1987, 1988; Romano & Zuccarello 2007) have only used the flare productivity of an AR to select a SAR, we also refer to an AR as a SAR, if the soft X-ray flare index is larger than 15.0 and any one of the other criterion conditions is met.

When applying all four criterion conditions, there are 45 SARs selected in solar cycles 21–23, which are listed in Table A.1 of Appendix A. Our sample includes 16 SARs from Bai (1988), 10 SARs from Wu & Zhang (1995), 12 SARs from Li & Wang (1997), 14 SARs from Tian et al. (2002), and 11 SARs from Romano & Zuccarello (2007). The SARs in the sample occupy 0.44% of all the ARs in the last three solar cycles but produced 44% of all the X class X-ray flares in the same time interval, i.e., 186 X class X-ray flares. The productivity is 4.13 X class flares per SAR, which is two orders of magnitude larger than the productivity of an average AR.

There are 12 SARs in our list, which were covered by the observation of the Large Angle Spectrometric Coronagraph onboard the Solar and Heliospheric Observatory (SOHO/LASCO). From the SOHO/LASCO CME catalogue, we find that among the 12 SARs, five of them are associated with fast CMEs of velocity larger than 2000 km s^{-1}, six SARs contained CMEs with velocity of 1500–2000 km s^{-1} or closing to 1500 km s^{-1}, and one SAR event happened during a SOHO/LASCO data gap. This means that almost all the SARs are likely to produce very fast CMEs with velocity larger than 1500 km s^{-1}. Since the CMEs initiated in an AR manifest the magnetic properties not only of the AR itself, but also the large-scale magnetic field where the AR originate (Zhou et al. 2006), we intend in future studies to include the CME velocity as a new criterion parameter to quantify the SARs.

Since the parameters used to quantify SARs should be independent, we examine the bilateral correlations between each pair of the parameters and present our results in Figs. 1a–e. A t-test is used to examine the confidence level for each correlation coefficient. It can be seen that the linear correlation coefficients of the 10.7 cm radio peak flux with the maximum sunspot area and the short-term ΔTSI with the soft X-ray flare index are comparatively low (Figs. 1a,b), with values of 0.005 (confidence level <50%) and −0.18 (confidence level <80%), respectively. The linear correlation coefficients of both the maximum sunspot area and the 10.7 cm radio peak flux with the soft X-ray flare index (Figs. 1c,d) are 0.37, above the confidence level of 98%. We note that the linear correlation coefficient of the short-term ΔTSI with the maximum sunspot area is relatively high, with the value −0.52, above the 99.9% level of confidence (Fig. 1e), but we can see that the plot of these data is considerable scattered. Furthermore, we find that some ARs have very large sunspot areas, but that the short-term ΔTSI caused by them are very low, for example AR 3776. In contrast, some ARs have very small sunspot areas, but the short-term ΔTSI caused by them are very high, as in the case of AR 5533. The linear correlation coefficient of the 10.7 radio peak flux with the short-term ΔTSI is −0.082 (confidence level <50%), which is also very low. On the basis of Figs. 1a–e, we can conclude that there are linear correlations between some pairs of the parameters to a certain extent. However, these correlations are not very tight, and neither of them can be substituted by another. Thus, all the aforementioned parameters need to be considered in this analysis.

We also surveyed the relationship between the CME velocities and the soft X-ray flare index of the 11 SARs that occurred during the period covered by the CME catalogue (Fig. 1f). It can be seen that there is a linear correlation between them, with the corresponding linear correlation coefficient 0.66, which is above the 95% level of confidence. However, the plot of these data also displays considerable scatter (see the discussion by Chen & Zong 2009). Both CMEs and flares may be produced by quite different mechanisms (Feynman & Hundhausen 1994) or the same mechanism but two different components of explosive magnetic-energy release (Jain et al. 2010). The linear correlations between the CME velocities and the other three criterion conditions are even weaker.

3. Statistical properties of SARs

Many authors have tried to parameterize SARs (Bai 1988; Wu & Zhang 1995; Li & Wang 1997; Tian et al. 2002; Romano & Zuccarello 2007), but each of them have used different sets of criterion conditions, thus obtained different SAR lists for the same time interval. As there are no soft X-ray flare and total solar irradiance data available, we cannot parameterize SARs in solar cycles 19 and 20 using the above four criterion conditions. To extend the sample, we consider 165 ARs, including the SARs studied by the above authors and selected by ourselves in solar cycles 19–23, to analyze the latitudinal and longitudinal distributions of SARs.

3.1. Latitudinal distribution of SARs

Figure 2 shows the latitudinal distribution of these 165 SARs. In this figure, each circle represents a SAR. Black-filled circles denote the SARs selected both by other authors and by ourselves, open circles are the SARs selected only by other authors, gray-filled circles represent the SARs selected only by ourselves, and the lines delineate the mean latitude of sunspots. We found that the latitudinal distribution of SARs for the northern (positive latitude) and southern (negative latitude) hemispheres resemble

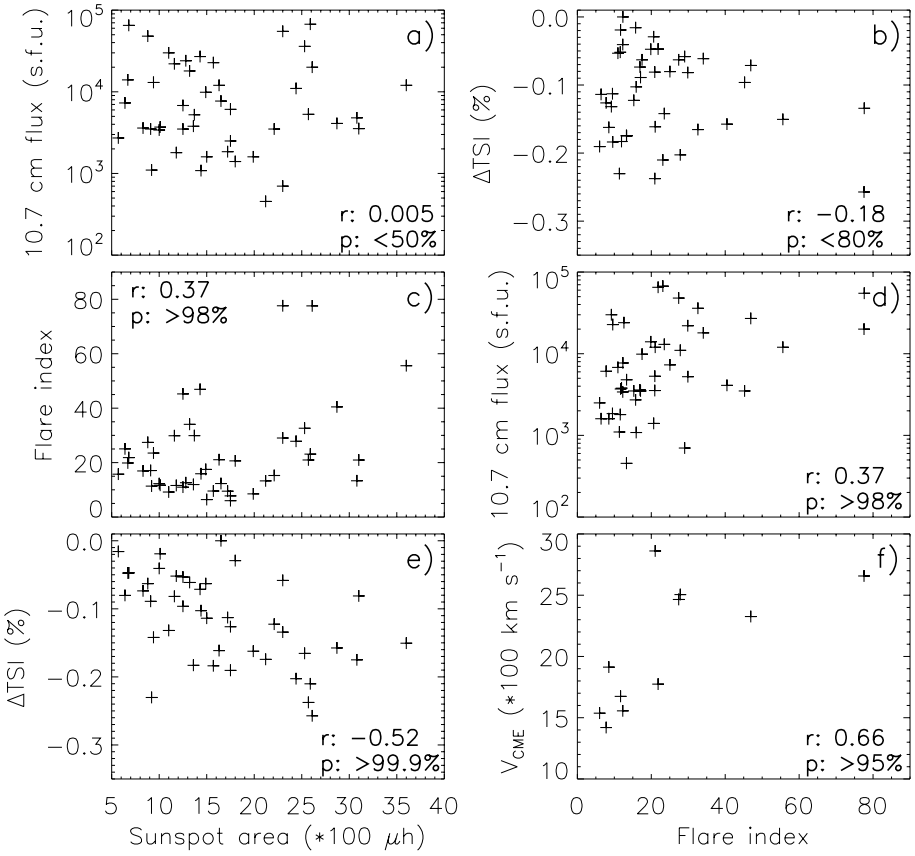

Fig. 1. Scatter plots of the 10.7 cm radio peak flux versus the maximum sunspot area **a**), the short-term ΔTSI versus the soft X-ray flare index **b**), the soft X-ray flare index versus the maximum sunspot area **c**), the 10.7 cm radio peak flux versus the soft X-ray flare index **d**), ΔTSI versus the maximum sunspot area **e**), and the CMEs velocities versus the soft X-ray flare index **f**). The symbol ***r*** is the linear correlation coefficient and ***p*** is the confidence level.

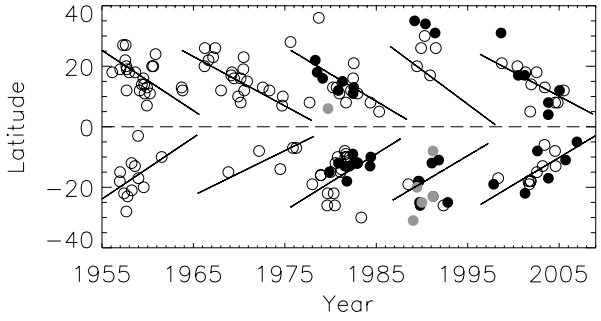

Fig. 2. The latitudinal distribution of SARs for the northern (positive latitude) and southern (negative latitude) hemispheres in solar cycles 19–23. Black-filled circles denote the SARs selected both by other authors and by ourselves, open circles denote the SARs selected only by other authors, gray-filled circles denote the SARs selected only by ourselves, and the lines denote the mean latitude of sunspots.

Maunder butterfly diagrams, which describe the latitudinal distribution of sunspots. At the same time, we can see that there are some differences between the distribution of SARs and that of ordinary sunspots. Few SARs appeared in the beginning and ending phases of each solar cycle, i.e. SARs occur preferentially in the maximum period of each solar cycle.

We also study the N-S asymmetry of SARs. The N-S asymmetry index ($A_{\rm NS}$) is defined as

$$A_{\rm NS} = \frac{N - S}{N + S}, \tag{1}$$

where N and S are the number of SARs in the northern and southern hemispheres of each solar cycle, respectively. Since the probability of either missing or misidentifying a SAR is not very high, we assume that the uncertainty in the identified SAR numbers is 1, hence that according to the error transfer theorem, the error of $A_{\rm NS}$ is $2/(N+S)$. The $A_{\rm NS}$ for SARs in the five solar cycles, cycles 19–23, are 0.31 ± 0.06, 0.62 ± 0.08, −0.18 ± 0.04, −0.30 ± 0.09, and 0.00 ± 0.06, respectively. It can be seen that SARs occurred primarily in the northern hemisphere during solar cycles 19 and 20 and the southern hemisphere during solar cycles 21 and 22. These results confirm those of Verma (2000), who studied the N-S asymmetry of solar active phenomena including sunspot areas, solar flares, and solar active prominences. They also found that the solar active phenomena are northern dominated in solar cycles 19 and 20 and southern dominated in solar cycles 21 and 22. However, SARs and solar active phenomena have different N-S asymmetry behaviors in solar cycle 23, SARs being almost equally distributed between both hemispheres, but solar active phenomena being primarily found in the southern hemisphere (Verma 2000). The SARs selected by ourselves (black-filled circles and gray-filled circles) have a behavior similar to that of all the SARs. Other authors (Garcia 1990; Li et al. 1998; Joshi et al. 2010) studied the N-S asymmetry of major flares and found a similar N-S asymmetry between their spatial distributions as Verma (2000).

3.2. Longitudinal distribution of SARs

We usually assume that the rotation period of the Sun is given by a Carrington rotation (CR) period (in sidereal frame 25.38 days and in synodic frame 27.2753 days) and measure the longitude of AR in the Carrington frame. However, the Sun does not rotate as a rigid body and its rotation is quite complicated.

To study the longitudinal distribution of SARs, we used a similar method as the method of Bai (1987, 1988), assuming that the rotation period of the Sun is P, and that the migration of the longitude of a SAR relative to the Carrington longitude is

$$\Delta L = (t/P - t/T_{\rm c}) \times 360, \tag{2}$$

where t is the time elapsed since 00:00 UT on 1956 January 1 and T_c is the synodic CR period. The relative longitude of a SAR in this frame is expressed by

$$L_r = L_c - \Delta L - n \times 360, \tag{3}$$

where L_c is the observed longitude of the SAR in the Carrington frame and n is defined to ensure that L_r remains within the range [0°, 360°].

If the number of SARs in ith CR is N_i, the normalized number of the kth SAR in this CR is defined as

$$N_{ik} = \frac{1}{N_i}. \tag{4}$$

We define the variance in the longitudinal distribution to be

$$V = \frac{1}{360}\sum_{j=0}^{359}(N_j - \overline{N})^2, \tag{5}$$

where N_j is the normalized number of SARs in a 30° longitude interval centered around j° and $\overline{N}$ is the mean of N_j. The variance provides a measure of the uniformity of the SAR distribution. If the distribution of SARs is perfectly uniform, V will be zero. The larger the variance V is, the less uniform the distribution of SARs.

Many authors have found that ARs occur preferentially at certain longitudes (Švestka 1970; Dodson & Hedeman 1975a; Tian et al. 2002). According to the SAR family trees identified in Bai (1987, 1988), the rotation periods of SARs are shorter than the Carrington period in both the northern and southern hemispheres. In this paper, we varied the value of P in the interval [23.0, 27.5] in steps of 0.01, hence the optimum value of P can be obtained when the maximum variance V is found. Owing to the N-S asymmetry of SARs, we analyzed the SARs in the northern and southern hemispheres separately. The rotation periods of SARs in the northern and southern hemispheres are 26.72 and 26.84, respectively. The northern hemisphere synodic rotation period is the same as the result of Bai (1988). However, the synodic rotation period in the southern hemisphere is larger than the result of Bai (1988) of 26.61 days.

Figure 3 shows the normalized number distribution of SARs for the relative longitudes in a 20° longitude interval in the northern (upper panel) and southern (lower panel) hemispheres. In this figure, the normalized number has been smoothed and the width of the smoothing window is 80°. We can see that there are two active longitudes, a primary longitude and a secondary longitude, which are about 160°–200° apart (black lines). The SARs selected by ourselves have a similar distribution (gray lines). Our independent examination confirms the conclusions drawn by Berdyugina & Usoskin (2003) and Usoskin et al. (2005).

On the basis of the uncertainty in our statistical study, we assumed that there are two persistent active longitudes, about 180° apart. We used an improved dynamic reference frame (Zhang et al. 2008, 2011) inferred from the differential rotation on the Sun to calculate the rotation parameters of SARs and study the longitudinal distribution of SARs in this frame. This frame relates an angular velocity Ω (deg/day) to a latitude φ as

$$\Omega = \Omega_0 - B\sin^2\varphi, \tag{6}$$

where Ω_0 (deg/day) is the equatorial angular velocity and B describes the differential rotation rate. Throughout our analysis for this paper, we used the CR period as the time step, for which Eq. (6) takes the form

$$\Omega_i = \Omega_0 - B\sin^2\varphi_i, \tag{7}$$

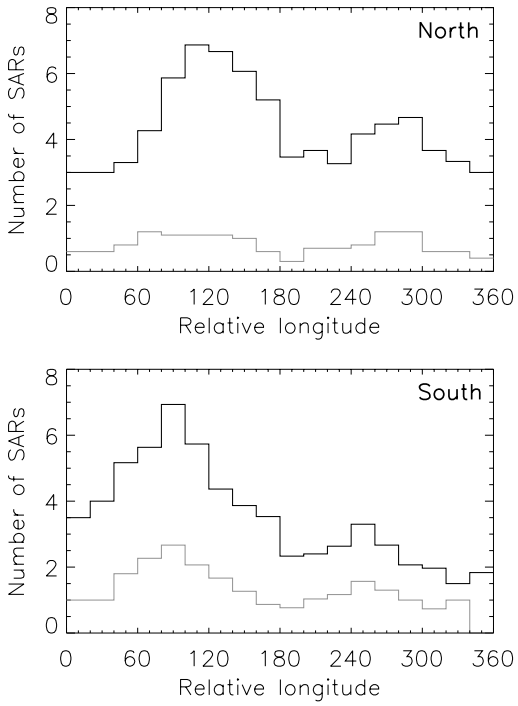

Fig. 3. The normalized number distribution of SARs for the relative longitudes in the northern (*upper panel*) and southern (*lower panel*) hemispheres. The black lines denote all the SARs and the gray lines denote the SARs selected by ourselves.

where index i denotes the ith CR, Ω_i (deg/day) is the same angular velocity as Ω in Eq. (6), and φ_i is the average latitude of SARs during this CR. For CRs without SARs, we use linear interpolation to get the mean latitude. Based on that, on the kth day of the ith CR, the migration of a longitude according to the solar surface differential rotation law is described as

$$M = T_c\sum_{i=N_0}^{N_{i-1}}(\Omega_i - \Omega_c) + k(\Omega_i - \Omega_c), \tag{8}$$

where N_0 and N_{i-1} denote the number of the initial and $(i-1)$th CR, respectively, and Ω_c is the angular rotation rate of Carrington system (in sidereal frame 14.1844 deg/day and in synodic frame 13.199 deg/day).

We assumed that one active longitude band is at Λ_{01} at the beginning and at Λ_{ik1} on the kth day of the ith CR, respectively. Using the above migration, we were able to obtain

$$\Lambda_{ik1} = \Lambda_{01} + M - n \times 360°, \tag{9}$$

where n is defined such that Λ_{ik1} remains within the range [0°, 360°]. The other active longitude band is at $\Lambda_{ik2} = \Lambda_{ik1} \pm 180°$ on the kth day of the ith CR. In the new reference frame, the longitude of a SAR, which occurs on the kth day of the ith CR, is defined as

$$\widetilde{L_{ik}} = L_{ik} - M - n \times 360°, \tag{10}$$

where L_{ik} is the observed longitude of the SAR in the Carrington frame.

The minimum difference between the longitude position of a SAR, L_{ik}, and the active longitude band, Λ_{ik1} or Λ_{ik2}, is

$$\delta_{ik} = \min(|L_{ik} - \Lambda_{ik1}|, 360° - |L_{ik} - \Lambda_{ik1}|, |180° - |L_{ik} - \Lambda_{ik1}||). \tag{11}$$

The mean deviation is defined as

$$\varepsilon = \frac{1}{N}\sum_i\sum_k N_{ik}\delta_{ik}^2, \tag{12}$$

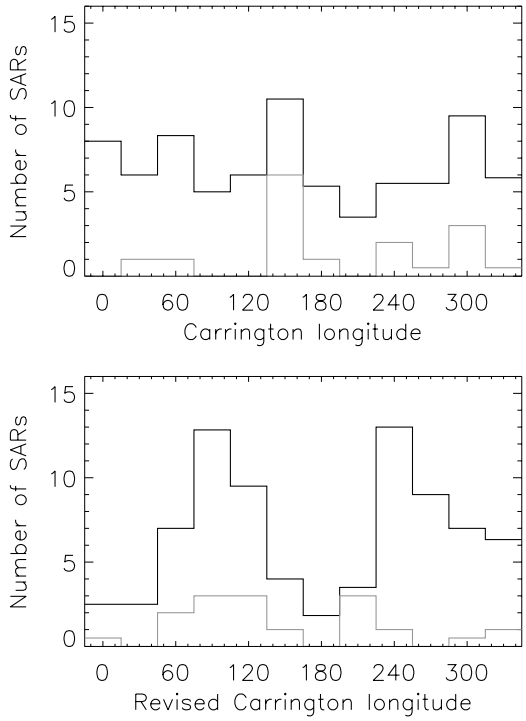

Fig. 4. The normalized number distribution of SARs in the Carrington frame (*upper panel*) and in the new dynamic reference frame (*lower panel*) during solar cycles 19–23 in the northern hemisphere. The black lines denote all the SARs and the gray lines denote the SARs selected by ourselves.

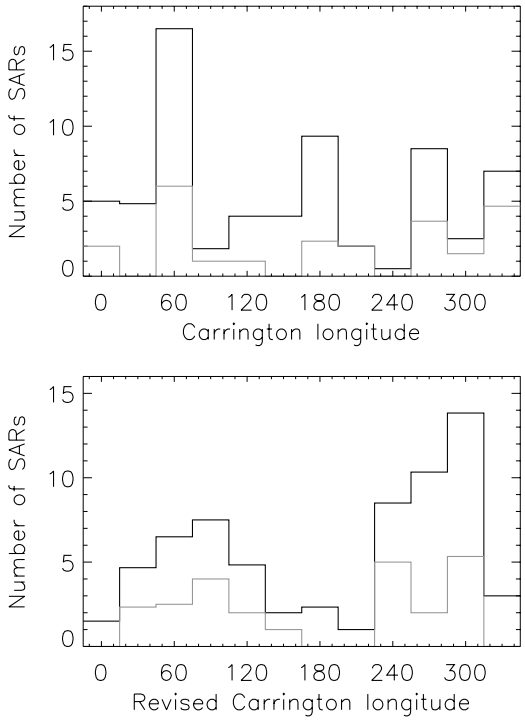

Fig. 5. The same as Fig. 4 but for the southern hemisphere.

where N is the total normalized number of SARs. We varied the value of Ω_0 in the interval [13.5, 15.0] in steps of 0.01, B in [1.0, 5.0] in steps of 0.01, and Λ_{01} in [0°, 180°] in steps of 1°. The best-fit parameters, Ω_0 and B, can be obtained when the minimum mean deviation ε is found.

The best-fit parameters are $\Omega_0 = 14.61 \pm 0.01$ and $B = 4.48 \pm 0.04$ for the northern hemisphere, and $\Omega_0 = 14.59 \pm 0.01$ and $B = 4.60 \pm 0.06$ for the southern hemisphere. Using these parameters, we found that the synodic rotation period and the sidereal rotation period, respectively, are 27.19 days and 25.30 days for the northern hemisphere, and 27.25 days and 25.36 days for the southern hemisphere at the latitude of 17°. From these results, we also can see that the rotation period of SARs is shorter than the CR period.

Figure 4 shows the number distribution of SARs for the observed (upper panel) and revised (lower panel) Carrington longitudes, which are binned by 30°, during solar cycles 19–23 in the northern hemisphere. In this figure, for display purposes, we assume two active longitude bins of Λ_{01} and $\Lambda_{01} + 180°$ at 90° and 270°. We note that most of the SARs are not exactly at the preferred longitudes in the upper panel, but tend to cluster around the two active longitudes bands, 90° and 270°, in the lower panel (black lines). The SARs selected by ourselves have a similar distribution (gray lines). A similar phenomenon is found in the southern hemisphere (Fig. 5). To quantify the character of SARs occurring preferentially at the two active longitudes, we calculate the non-axisymmetry in the number distribution of SARs as

$$N_1 = \sum_{i,k} N_{ik}, \quad \text{if} \quad \delta_{ik} < 45°,$$
$$N_2 = \sum_{i,k} N_{ik}, \quad \text{otherwise}, \tag{13}$$

where N_1 and N_2 represent the total normalized number of SARs that occurred close to and far from the two active longitude bands, respectively. The non-axisymmetry is defined as

$$\Gamma = \frac{N_1 - N_2}{N_1 + N_2}. \tag{14}$$

The magnitudes of the non-axisymmetry for SARs are 0.48 and 0.56 in the northern and southern hemispheres, respectively. This implies that 74% and 78% ($N_1/(N_1 + N_2)$) of the SARs occurred near one of the two active longitudes in the northern and southern hemispheres, respectively. This result is consistent with the results of Zhang et al. (2007a,b, 2011).

4. Conclusions and discussion

We have re-parameterized the SARs in solar cycles 21–23 using the following four criterion conditions (see Table 1): the maximum sunspot group area, the soft X-ray flare index, the 10.7 cm radio peak flux, and the short-term ΔTSI. If three of these four criterion conditions are met, an AR is called a SAR. For an extreme flare-prolific AR, if the soft X-ray flare index is larger than 15.0 and any one of the other criterion conditions is met, it is also called a SAR. There are 19 SARs selected in solar cycle 21, 14 SARs in solar cycle 22, and 12 SARs in solar cycle 23. These 45 SARs occupy 0.44% of all the ARs in the last three solar cycles but produced 44% of all the X class X-ray flares in the same time interval. The SARs are likely to be associated with very fast CMEs with velocity larger than 1500 km s^{-1}.

The bilateral linear correlations between each pair of the four parameters used to parameterize the SARs were examined in this paper. It was found that all the four parameters are independent to a certain extent and it is reasonable to parameterize SARs based on these four parameters.

The geomagnetic A_p index and the high-energy proton flux (≥10 MeV) had previously been used to parameterize SARs by other authors (Wu & Zhang 1995; Li & Wang 1997; Tian et al. 2002; Wang et al. 2011). It had also been noticed, however,

that strong geomagnetic storms and large high-energy proton fluxes are mostly caused by CMEs and depend on the position of the related ARs (Webb 1995; Crooker 2000; Webb et al. 2000; Yermolaev & Yermolaev 2002; Kocharov et al. 2007). These two parameters are not solely related to sunspot groups. On the other hand, the fast ($\geq$1000 km s^{-1}) or extremely fast ($\geq$2000 km s^{-1}) CMEs initiated in an AR seem to be more closely related to its magnetic property, e.g., its large-scale magnetic connectivity (Zhou et al. 2006), and should also be considered as a criterion parameter. Owing to the incompleteness of CME data coverage in the last three cycles, we have been unable to adopt the CME velocity as a criterion variable in these series studies. In the future, we intend to include it as a new criterion condition to parameterize SARs.

To extend the sample of SARs for a statistical study, we used 165 SARs that included the SARs referred to by other authors (Bai 1988; Wu & Zhang 1995; Li & Wang 1997; Tian et al. 2002; Romano & Zuccarello 2007) and analyzed the latitudinal and longitudinal distributions of all these SARs. We found that the latitudinal distribution of SARs resembles Maunder butterfly diagrams and that SARs occur preferentially during the maximum period of each solar cycle, which is consistent with the conclusion of Jiang et al. (2011). However, Švestka (1995) found that larger flares tend to occur during the declining phase of the sunspot cycle. The SARs occurred primarily in the northern hemisphere in solar cycles 19 and 20 and the southern hemisphere in solar cycles 21 and 22. However, about equal numbers of SARs occurred in each hemisphere during solar cycle 23. There are some differences in the N-S asymmetry between SARs and solar active phenomena. The solar active phenomena are northern dominated in solar cycles 19 and 20 and southern dominated in solar cycles 21–23 (Garcia 1990; Li et al. 1998; Verma 2000; Joshi et al. 2010). As other authors had found, there are two active longitudes on the Sun, about 160°–200° apart (Berdyugina & Usoskin 2003; Usoskin et al. 2005).

Based on the differential rotation on the Sun, we have applied an improved dynamic reference frame (Zhang et al. 2008, 2011) to SARs. We have found that the synodic rotation period and the sidereal rotation period of SAR are 27.19 days and 25.30 days in the northern hemisphere, and 27.25 days and 25.36 days in the southern hemisphere. The SARs rotate slightly more rapidly in the northern hemisphere than in the southern hemisphere, but there is no significant difference between the two hemispheres. The rotation period of SARs in the dynamic reference frame is shorter than the Carrington period in both the northern and southern hemispheres. However, Zhang et al. (2007a, 2011) found that the average flare rotates significantly differently in the two hemispheres, with flares rotating faster and slower than the Carrington rate in the northern and southern hemispheres, respectively.

We also found that the non-axisymmetries of SARs in the longitudinal distribution are significant in both the northern and southern hemispheres. About 75% of the SARs occurred near two active longitudes with half widths of 45°. Using these results, we have been able to predict the two active longitudes. If an AR occurs near one of the two active longitudes, we might be expected to detect enhanced activity.

The characteristics of a SAR vector magnetic field are of great help in understanding the physics explaining why SARs are extremely active and characterizing the activity of each solar cycle. In future work, we will use the vector magnetic field data of the photosphere taken by the Solar Magnetic Field Telescope at Huairou Solar Observatory Station to survey the vector magnetic field characteristics of these SARs.

Acknowledgements. The authors thank Dr. H. M. Wang and Dr. L. Y. Zhang for useful discussions, and thank Dr. J. Jiang for valuable suggestions. Thanks are also due to Dr. H. Peter and the anonymous referee for their valuable suggestions, which improve the manuscript greatly. The research is supported by the National Natural Science Foundation of China (10873020, 40974112, 40890161, 11025315, 10921303, 10703007 and 40804030) and the National Basic Research Program of China (2011CB811403).

References

Ashish, G., & Choudhuri, A. R. 2009, Res. Astron. Astrophys., 9, 115
Bai, T. 1987, ApJ, 314, 795
Bai, T. 1988, ApJ, 328, 860
Balachandran, B., Lanzerotti, L. J., & Gary, D. E. 2001, AGU, Fall Meeting, abstract #SH31A-0629
Berdugina, S. V., & Usoskin, I. G. 2003, A&A, 405, 1121
Chen, A.-Q., & Zong, W.-G. 2009, Res. Astron. Astrophys., 9, 470
Covington, A. E. 1959, Proc. IAU Symp., 9, 159
Covington, A. E., & Harvey, G. A. 1958, JRASC, 52, 161
Crooker, J. U. 2000, J. Atm. Solar-Terrestrial Phys., 62, 1071
Dodson, H. W., & Hedeman, E. R. 1971, World Data Center for Solar-Terrestrial Physics Report UAG-14 (Boulder: NOAA)
Doddson, H. W., & Hedeman, E. R. 1975a, Sol. Phys., 42, 121
Dodson, H. W., & Hedeman, E. R. 1975b, World Data Center for Solar-Terrestrial Physics Report UAG-52 (Boulder: NOAA)
Dodson, H. W., & Hedeman, E. R. 1981, World Data Center for Solar-Terrestrial Physics Report UAG-80 (Boulder: NOAA)
Feynman, J., & Hundhausen, A. J. 1994, J. Geophys. Res., 99, 8451
Gaizauskas, V., Harvey, K. L., Harvey, J. W., & Zwaan, C. 1983, ApJ, 265, 1056
Garcia, H. A. 1990, Sol. Phys., 127, 185
Henney, C. J., & Harvey, J. W. 2002, Sol. Phys., 207, 199
Jain, R., Aggarwal, M., & Kulkarni, P. 2010, RAA, 10, 473
Jiang, J., Cameron, R. H., Schmitt, D., & Schüssler, M. 2011, A&A, 528, A82
Joshi, N. C., Bankoti, N. S., Pande, S., et al. 2010, New Astron., 15, 538
Kocharov, L., Saloniemi, O., Torsti, J., et al. 2007, ApJ, 659, 780
Li, W. B., & Wang, H. Z. 1997, Publ. Yunnan Obs., 1, 10
Li, K.-J., Schmieder, B., & Li, Q.-S. 1998, A&AS, 131, 99
Li, Y., Luhmann, J., Fisher, G., & Welsch, B. 2004, J. Atm. Solar-Terrestrial Phys., 66, 1261
Neugebauer, M., Smith, E. J., Feynman, J., et al. 2000, J. Geophys. Res., 105, 2315
Romano, P., & Zuccarello, F. 2007, A&A, 474, 633
Ruzmaikin, A., Feynman, J., Neugebauer, M., & Smith, E. J. 2001, J. Geophys. Res., 106, 8363
Sammis, I., Tang, F., & Zirin, H. 2000, ApJ, 540, 583
Solanki, S. K., & Flige, M. 2002, Adv. Space Res., 29, 1933
Švestka, Z. 1970, Space Res., 10, 797
Švestka, Z. 1995, Adv. Space Res., 16, 27
Tian, L. R., Liu, Y., & Wang, J. X. 2002, Sol. Phys., 209, 361
Usoskin, I. G., Berdyugina, S. V., & Poutanen, J. 2005, A&A, 441, 347
Verma, V. K. 2000, JA&A, 21, 173
Wang, J. X., Chen, A. Q., Feynman, J., et al. 2011, Proc. IAU Symp., 273, in press
Webb, D. F. 1995, Rev. Gephs. Suppl., 33, 577
Webb, D. F., Cliver, E. W., Crooker, N. U., et al. 2000, J. Geophys. Res., 105, 7491
Withbroe, G. L. 2009, Sol. Phys., 257, 71
Wu, M. C., & Zhang, Q. 1995, Publ. Yunnan Obs., 1, 1
Yan, X.-L., Qu, Z.-Q., Xu, C.-L., et al. 2009, RAA, 9, 596
Yermolaev, Y. I., & Yermolaev, M. Y. 2002, Cosmic Res., 40, 1
Zhang, L. Y., Cui, Y. M., He, H., et al. 2007a, Adv. Space Res., 40, 970
Zhang, L. Y., Wang, H. N., Cui, Y. M., & He. H. 2007b, A&A, 471, 711
Zhang, L. Y., Wang, H. N., & Du, Z. L. 2008, A&A, 484, 523
Zhang, L. Y., Mursula, K., Usoskin, I., & Wang, H. 2011, J. Atm. Solar-Terrestrial Phys., 73, 258
Zhou, G. P., Wang, J. X., & Zhang, J. 2006, A&A, 445, 1133

Appendix A: Table

Table A.1. The list of superactive regions.

NOAA	Lat. Long.	Date on the disk Y M D	Maximum area (μh)	Flare index	10.7 cm flux (s.f.u.)	ΔTSI (%)	CME velocity (km s^{-1})
1092	N23 L081	780423-0507	**1280**	**12.6**	**24000**	No data	
1203	N18 L175	780708-0721	**1370**	**29.9**	**5230**	No data	
1574	N17 L155	790214-0225	**1100**	9.2	**30000**	**−0.132**	
1994	N06 L198	790916-0927	**1180**	**11.6**	**1800**	−0.052	
2099	S14 L283	791105-1112	**1720**	9.5	**1848**	**−0.113**	
2776	N12 L174	801101-1114	**1440**	**15.91**	**1084**	**−0.103**	
2779	S11 L105	801105-1119	**2300**	**29.03**	700	−0.058	
3049	N15 L153	810414-0430	**1490**	**17.5**	**9880**	−0.063	
3234	S12 L294	810721-0803	**2120**	**13.28**	454	**−0.174**	
3390	S18 L339	811007-1019	**1570**	9.57	**22750**	**−0.184**	
3576	S14 L322	820126-0209	**1360**	**11.94**	**3784**	**−0.183**	
3763	S08 L086	820602-0615	**1250**	**45.24**	**3500**	−0.096	
3776	N13 L314	820611-0624	**3100**	**20.94**	**3539**	−0.081	
3804	N14 L322	820708-0722	**2870**	**40.47**	**4100**	**−0.158**	
4026	S11 L078	821211-1223	640	**25.04**	**7300**	−0.080	
4474	S13 L343	840421-0505	**2590**	**23.13**	**67210**	**−0.210**	
4492	S10 L358	840518-0531	670	**19.87**	**13999**	−0.048	
5312	S31 L306	890106-0120	**1800**	**20.64**	**1400**	−0.029	
5395	N34 L256	890305-0319	**3600**	**55.6**	**12000**	**−0.151**	
5533	S19 L073	890609-0620	920	**11.37**	**1100**	**−0.230**	
5629	S17 L075	890803-0817	**1320**	**34.07**	**18000**	−0.061	
5669	S17 L085	890829-0912	**3080**	**13.32**	**4800**	**−0.175**	
5698	S26 L220	890918-0929	**1250**	**10.97**	**6800**	−0.053	
5747	S27 L210	891014-1027	**1160**	**29.87**	**22000**	−0.082	
5852	S26 L028	891225-1231	**1500**	6.42	**1600**	**−0.114**	
6063	N34 L318	900511-0524	940	**23.51**	**13000**	**−0.142**	
6471	S12 L144	910125-0208	**2210**	**15.27**	**3500**	**−0.123**	
6538	S23 L342	910305-0317	910	**17.08**	**3500**	−0.089	
6545	S09 L287	910311-0322	830	**16.93**	**3600**	−0.074	
6555	S23 L188	910317-0331	**2530**	**32.62**	**36000**	**−0.166**	
6659	N31 L247	910601-0617	**2300**	**77.61**	**55000**	**−0.134**	
6891	S12 L184	911021-1102	**2570**	**20.96**	**5300**	**−0.238**	
7321	S24 L070	921025-1102	**1650**	**12.32**	**7700**	0	
8100	S20 L352	971028-1107	**1000**	**12.28**	**3400**	−0.041	1556
8307	N31 L035	980818-0831	570	**15.75**	**2720**	−0.016	Data gap
9077	N18 L310	000709-0719	**1010**	**11.68**	**3700**	−0.019	1674
9393	N18 L153	010324-0404	**2440**	**27.84**	**11000**	**−0.203**	2505
9415	S22 L359	010403-0416	880	**27.42**	**48000**	−0.063	2465
10069	S08 L299	020811-0824	**1990**	8.51	**1600**	**−0.162**	1913
10484	N04 L354	031018-1028	**1750**	6.01	**2500**	**−0.191**	1537
10486	S16 L284	031022-1105	**2610**	**77.56**	**20000**	**−0.257**	2657
10488	N08 L290	031027-1104	**1750**	7.78	**6100**	**−0.126**	1420
10720	N13 L179	050111-0123	**1630**	**21.06**	**12000**	**−0.161**	2861
10808	S11 L230	050907-0918	**1430**	**46.92**	**27000**	−0.071	2326
10930	S05 L009	061204-1218	680	**21.84**	**65000**	−0.047	1774

Notes. The parameter matching the criterion of SARs is indicated in boldface type.